Spatial constraints dictate glial territories at murine neuromuscular junctions

Monika S. Brill,[1] Jeff W. Lichtman,[2] Wesley Thompson,[3] Yi Zuo,[4] and Thomas Misgeld[1,5]

[1]Chair of Biomolecular Sensors, Center for Integrated Protein Science Munich at the Institute of Neuroscience, Technische Universität München, 80802 Munich, Germany
[2]Department of Molecular and Cellular Biology, Harvard University, Cambridge, MA 02138
[3]Institute for Neuroscience, University of Texas at Austin, Austin, TX 78712
[4]Department of Molecular, Cell and Developmental Biology, University of California, Santa Cruz, Santa Cruz, CA 95064
[5]Institute for Advanced Study, Technische Universität München, 85748 Garching bei München, Germany

Schwann cells (SCs), the glial cells of the peripheral nervous system, cover synaptic terminals, allowing them to monitor and modulate neurotransmission. Disruption of glial coverage leads to axon degeneration and synapse loss. The cellular mechanisms that establish and maintain this coverage remain largely unknown. To address this, we labeled single SCs and performed time-lapse imaging experiments. Adult terminal SCs are arranged in static tile patterns, whereas young SCs dynamically intermingle. The mechanism of developmental glial segregation appears to be spatial competition, in which glial–glial and axonal–glial contacts constrain the territory of single SCs, as shown by four types of experiments: (1) laser ablation of single SCs, which led to immediate territory expansion of neighboring SCs; (2) axon removal by transection, resulting in adult SCs intermingling dynamically; (3) axotomy in mutant mice with blocked axon fragmentation in which intermingling was delayed; and (4) activity blockade, which had no immediate effects. In summary, we conclude that glial cells partition synapses by competing for perisynaptic space.

Introduction

Glial cells mediate central functions in the nervous system. They contribute to action potential propagation, immune surveillance, and ionic homeostasis. Recent work has focused on the role of glial cells at the synapse, where these cells are now recognized as the third partner in a tripartite structure (Araque et al., 1999). At synapses, glial cells monitor neurotransmission, contain and clear released transmitter, and modulate synaptogenesis and plasticity (Eroglu and Barres, 2010). To accomplish these diverse functions, glial cells arrange themselves in a highly organized manner (Bushong et al., 2002; Nedergaard et al., 2003). Not surprisingly, alterations of glial morphology and arrangement are hallmarks of many neurological diseases (Lobsiger and Cleveland, 2007; Barres, 2008; Nave, 2010), and glial disruptions lead to synaptic dysfunction (Eroglu and Barres, 2010). Still, it remains largely unknown how glial cells establish and maintain their perisynaptic territories. This is because of the fact that central synapses are hard to access and too small to be resolved by conventional light microscopy. Moreover, simple methods to label individual glial cells suitable for intravital imaging have not been widely available (Bushong et al., 2002; Livet et al., 2007).

The neuromuscular junction (NMJ), because of its size and accessibility, offers an ideal site to study how glial cells establish perisynaptic territories. NMJs and their innervating axons are sheathed by axonal and terminal Schwann cells (SCs), with the first forming myelin and the second covering synaptic terminals (Sanes and Lichtman, 1999). Ultrastructural work has revealed that terminal SC processes are intimately associated with axon terminals, postsynaptic sites, and processes of neighboring glial cells (Desaki and Uehara, 1981). The glial coverage of developing NMJs is dynamic; initially, most murine NMJs have only one terminal SC, but proliferation rapidly adds additional cells (Love and Thompson, 1998). In adulthood, SC numbers remain stable (Zuo et al., 2004),

Y. Zuo and T. Misgeld contributed equally to this paper.

Correspondence to Thomas Misgeld: thomas.misgeld@lrz.tum.de; or Yi Zuo: yizuo@ucsc.edu

Abbreviations used in this paper: AAD, acute axonal degeneration; AChR, acetylcholine receptor; BoTX, botulinum toxin; BTX, bungarotoxin; CNS, central nervous system; EtHD, ethidium homodimer; NMJ, neuromuscular junction; SC, Schwann cell.

The Rockefeller University Press $30.00
J. Cell Biol. Vol. 195 No. 2 293–305
www.jcb.org/cgi/doi/10.1083/jcb.201108005

although slow changes in morphology have been documented (Livet et al., 2007). This picture changes dramatically after denervation, which leads to a reactive transformation of SCs, proliferation, and growth of processes (Birks et al., 1960; Miledi and Slater, 1968, 1970; Reynolds and Woolf, 1992; Son and Thompson, 1995a,b; O'Malley et al., 1999; Kang et al., 2003). In all these situations, SCs are essential for the maintenance, formation, and regeneration of NMJs. For example, ablation of all terminal SCs at frog NMJs leads to gradual retraction of axonal terminals and disrupts synaptogenesis (Reddy et al., 2003). Also, reactive SC processes are critical for guiding regenerating axons back to synaptic sites (Son and Thompson, 1995a,b; Nguyen et al., 2002; Kang et al., 2003). Despite the importance of proper glial coverage of NMJs, many questions remain unanswered. What is the territory of individual terminal SC under normal conditions? How is this territory established during development, and what mechanisms maintain it? How do single SC territories change after axonal degeneration, and which signals drive these changes?

To address these questions, we have devised methods to differentially label single SCs, taking advantage of sequential dye filling and photobleaching in transgenic mice with GFP-labeled SCs (SC-GFP mice; Mallon et al., 2002; Zuo et al., 2004). This allowed us to reveal that mature SCs occupy segregated territories. This segregation is absent during development, lost after denervation, and swiftly restored after reinnervation. Laser ablation of single SCs and axons revealed that the territory of a single terminal SC is constrained by spatial competition with its glial neighbors and its underlying axon terminal but not by axonal transport or activity.

Results

Mature SCs occupy segregated territories

Because of direct apposition between terminal SCs, no clear borders between individual cells could be defined in NMJs of SC-GFP mice by conventional confocal microscopy alone (Figs. 1 [A and B] and S1). To delineate individual SC territories, we developed two independent techniques (for details, see Materials and methods): we either sequentially dye filled individual SCs with rhodamine dextran (Fig. S1 A) or used sequential photobleaching (Fig. 1, A and B). Three types of SC contacts became apparent (Fig. S1): contacts that involved axonal SCs (axonal–axonal and axonal–terminal) and contacts between terminal SCs (terminal–terminal). Axonal SCs were delineated by gaps indicative of nodal structures, which were surrounded by immunoreactivity for the paranodal marker contactin associated protein-1 (Caspr; Fig. S1 B; Scherer, 1996). A heminode, with unilateral Caspr immunoreactivity, defined the synaptic entry point and was never crossed by glial processes (Fig. S1 B; $n > 70$ terminal SCs and 7 axonal SCs that participated in a heminode). Within the synapse (where Caspr accumulations are absent), single-cell labeling also revealed clearly defined glial territories that tile the mature NMJ (Figs. 1 B and S1 [A and B]). Mature terminal SCs possess multiple processes (sternomastoid: 4.9 ± 0.4 per cell, $n = 32$ SCs, 12 muscles; triangularis sterni: 4.4 ± 0.2, $n = 31$ SCs, 7 muscles) that show almost no overlap at SC–SC contact sites (Fig.1 C). Despite these sharp boundaries, extensive cell–cell contacts and, hence, potential communication sites between neighboring SCs exist. When we coinjected a small molecular tag (neurobiotin; ∼300 D; Kristan et al., 2000) together with rhodamine dextran, we found that terminal SC pairs were coupled at 59% of NMJs ($n = 10/17$ NMJs, 17 muscles; Fig. S1 C), compatible with the presence of gap junctions. In contrast, coupling between terminal and axonal SCs was never observed ($n = 0/9$ NMJs, nine muscles). Thus, in undisturbed adult NMJs, terminal and axonal SCs belong to distinct compartments. Individual terminal SCs cover distinct synaptic territories but at the same time can form a functional syncytium, which might allow for intercellular signaling.

Immature SCs intermingle

The presence of well-delineated adult SC territories could arise from two developmental scenarios: SC territories could already be segregated at immature NMJs, as SCs emerge in a sequential fashion by local proliferation (Love and Thompson, 1998; Jessen and Mirsky, 2005), and, alternatively, SC territories could initially be intermingled and sort out as development proceeds, similar to axonal segregation during synapse elimination (Gan and Lichtman, 1998). Single-cell labeling allowed us to distinguish between these scenarios.

The morphology of immature terminal SCs at postnatal days 7–11 (P7–11) differed dramatically from mature SCs. First, immature terminal SCs had a fried egg shape (Figs. 1 A and S2) compared with the branched morphology of mature SCs (Figs. 1 B and S1). These morphological differences of SCs correspond to the concurrent postsynaptic plaque-to-pretzel transition (Marques et al., 2000). Second, in contrast to the mature tile pattern, SCs in young animals were highly intermingled on the NMJ. For example, the degree of overlap between SC processes was much higher in immature NMJs compared with the adult (Fig. 1 C). In many cases, the processes of one SC projected underneath the processes or cell body of their neighbors (e.g., Fig. 1 A), a configuration rarely observed in adult NMJs. To quantify the overall degree of glial segregation, we determined the relative distance of the fluorescent centroids of single terminal SCs (Fig. 1, D and E; Gan and Lichtman, 1998). Adult SCs showed a higher degree of segregation than their immature predecessors. This segregation of glial cells is reminiscent of the sorting process of axon terminals at multiply innervated NMJs, which takes place at the same time of development (Gan and Lichtman, 1998) and is driven by glial digestion of intrasynaptic branchlets (Bishop et al., 2004). However, we did not find a match between glial and axonal territories when we used combined axonal (Turney and Lichtman, 2008) and SC bleaching to concomitantly reveal individual neuronal and glial territories (Fig. S2).

Immature SCs are highly dynamic but later settle down

The difference in morphology between immature and adult terminal SCs raises the question whether changes in cellular dynamics accompany this remodeling and perhaps accomplish it.

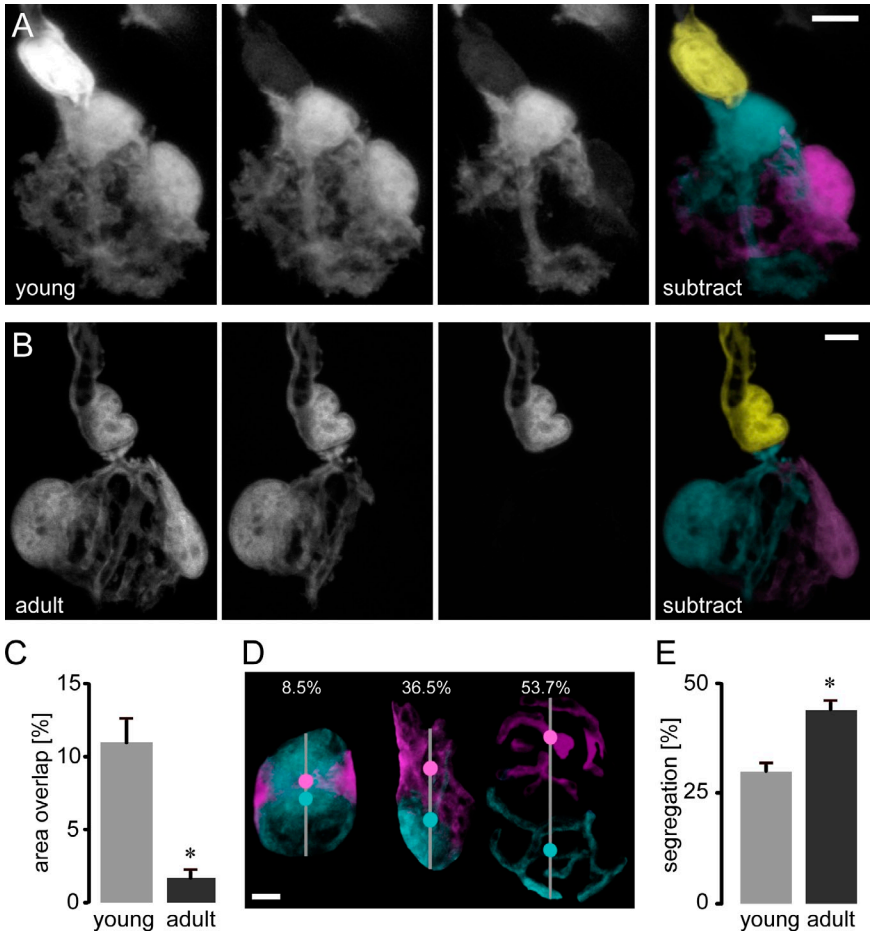

Figure 1. **Mature segregated terminal SC territories develop from initial glial intermingling.** (A and B) Sequential photobleaching of terminal SCs in P11 young (A) and adult (B) nerve–muscle explants from SC-GFP mice. Sequential bleaching steps are depicted in the middle two panels; subtracted and pseudocolored merges of confocal images are shown in the rightmost panels. (C) Terminal SC area overlap as a percentage of total synaptic (BTX positive) area (young: 11.0 ± 1.5%, n = 30 SC pairs, 10 triangularis sterni muscles; adult: 1.7 ± 0.4%, n = 26 SC pairs, 9 triangularis sterni muscles; *, $P < 0.01$ using a t test; data are represented as the mean of SC pairs + SEM). (D and E) Terminal SC segregation at young versus mature ages. (D) Three examples are shown: an extensively intermingled young SC pair (8.5% minimum), an intermediate example (36.5%), and a mature highly segregated terminal SC pair (53.7%; maximum segregation index measured). Color-coded dots indicate centroids of individual SCs, and lines indicate the length of the NMJ at the axis through the centroids. (E) Quantification of age-dependent segregation (calculated as the distance of the centroids over the length of the NMJ): young (P7–11; 30.4 ± 1.6%, n = 24 SC pairs, six triangularis sterni muscles) versus adult (44.6 ± 1.3%, n = 23 SC pairs, three triangularis sterni muscles; mean of SC pairs + SEM; *, $P < 0.01$ using a t test). Bars, 5 µm.

Although dynamic remodeling is necessary to transition from an intermingled to a tiled morphology, the degree of such dynamism is hard to predict from static images. Moreover, cells can tile territories either by establishing static segregated domains or by dynamic homotypic repulsion (Sagasti et al., 2005). To address this, we combined photobleaching with confocal time-lapse analysis of acute explants of triangularis sterni muscles of different ages (Kerschensteiner et al., 2008).

Immature terminal SCs rapidly formed and retracted cytoplasmic protrusions (Fig. 2 [A–C] and Video 1). These protrusions extended within the synapse, exploring the territory covered by a neighboring SC but also areas beyond the synaptic border. Similar outgrowth of axons has been described for young NMJs (Walsh and Lichtman, 2003), but when we concomitantly imaged axons and SCs at immature NMJs, no clear relationship between their protrusions was apparent (Video 1). Terminal SCs extended processes along the axon that innervates the synapse (unpublished data). At the same time, axonal SCs explored synaptic territory (Fig. S3), suggesting that at early developmental ages, there is no barrier to SC growth across the synaptic entry point.

The dynamism of immature SCs contrasted markedly to the behavior of mature SCs. Mature SC territories were highly stable when followed over periods of a few hours (Fig. 2, D–F). At best, minute protrusions extended transiently into the territory covered by a neighboring cell but immediately withdrew (Fig. 2 F and Video 2). Similarly restricted growth was also apparent across the terminal heminode, both from within the synapse toward the axon and vice versa (Fig. S3). At the same time, adult SCs did not extend processes away from their axon (n = 0/14 SCs, six triangularis sterni explants). We compared the total area sampled by individual terminal SCs over time with their own mean size (Fig. 2, G–J). Immature SCs sampled three times larger relative territories over the same period of time compared with their mature counterparts (Fig. 2 H). On average, SCs did not change in net size over the observation period (Fig. 2, I and J), ruling out phototoxic damage as a likely explanation for the described dynamism.

Our ex vivo observations of limited adult SC dynamism over periods of hours did not rule out that bigger changes would arise over months (Livet et al., 2007). To address this possibility, we performed long-term observations of single NMJs using repetitive in vivo imaging in the sternomastoid muscle (see Materials and methods; Fig. 3; Lichtman et al., 1987; Zuo et al., 2004). Indeed, we found significant long-term remodeling of terminal SCs in the adult. Out of 53 adult NMJs (n = 10 mice) followed over several weeks, more than one third showed obvious changes in terminal SC position or number, such as translocation (13%), disappearance (15%), or addition (15%). Sequential bleaching further revealed that newly added terminal SCs obtained substantial synaptic territory from their neighbors (Fig. 3 B).

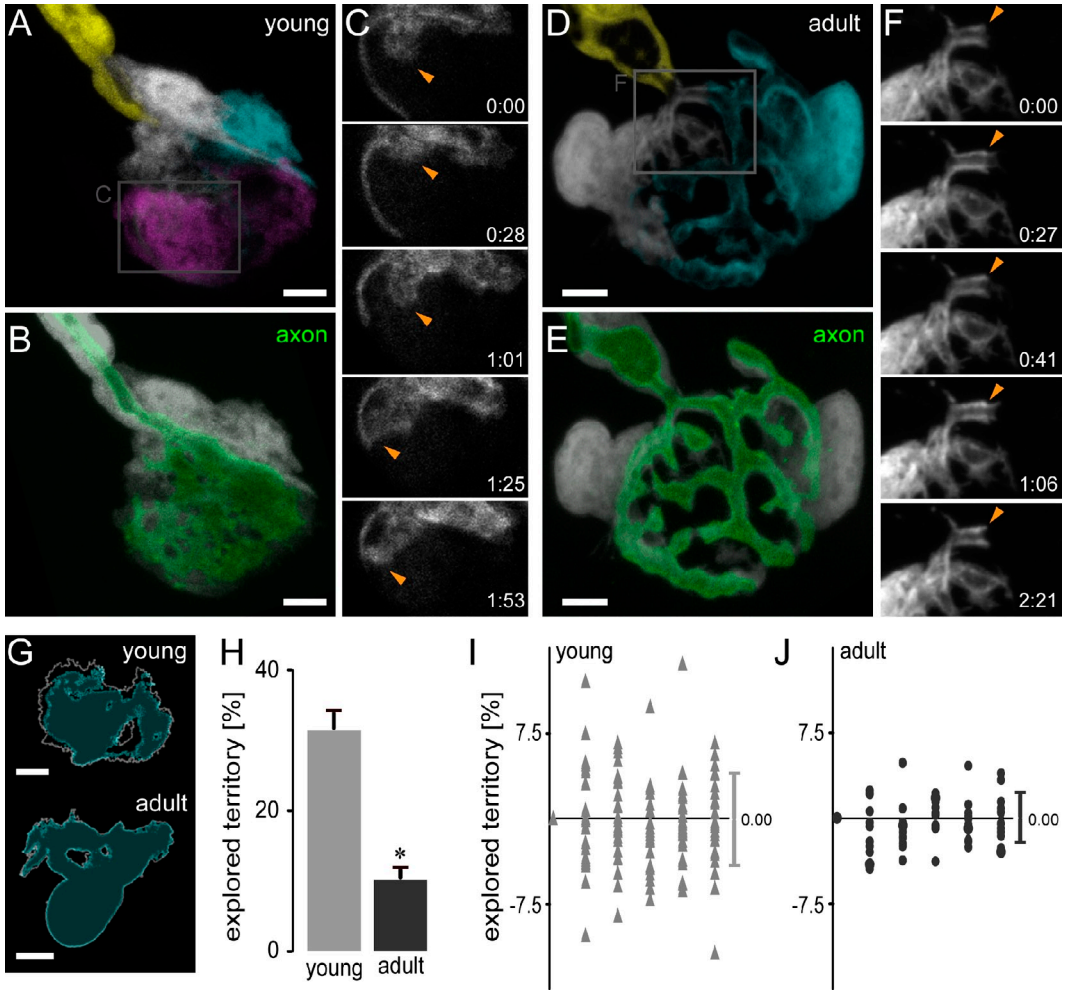

Figure 2. **Immature SCs are highly dynamic, whereas adult SCs are static.** (A–F) Confocal time-lapse microscopy of young (A–C) and adult (D–F) SC-GFP terminal SCs in nerve–muscle explants. (A and D) Sequentially bleached young (A) and adult (D) NMJs with pseudocolored terminal and axonal SCs. (B and E) NMJ labeled for axons (*thy1*-Membow13) and SCs (white). (C and F) Time-lapse recordings over ∼2 h (areas boxed in A and D). Immature terminal SCs were highly dynamic (C; arrowheads), whereas only minor growth or retraction was observed in the adult (F), especially at contact sites with neighboring cells (arrowheads). (G and H) Quantitative analysis of SC dynamism. (G) Example of individual young and adult terminal SC showing mean area covered (cyan) and maximum territory covered (white outline). (H) Quantification of explored territory within 1 h (young: 31.4 ± 2%, n = 24 individual SCs, eight triangularis sterni explants vs. adult: 10.2 ± 1%, n = 14 individual SCs, six triangularis sterni explants; values are normalized to terminal SC size; *, $P < 0.001$ using a t test; data are represented as the mean of SCs + SEM). (I and J) Territory exploration plotted over a period of 1 h for young (I) and adult (J) terminal SCs (territory difference per 10 min plotted; bars on the right show the mean ± SD; total territories stay stable for 1 h; change −0.45 µm^2 for young and −0.28 µm^2 for adult terminal SCs, shown normalized to SC size in the figure). The timers shown represent hours/minutes. Bars, 5 µm.

SC territories are restricted by neighboring SCs

What determines how SCs partition NMJs at different developmental stages? Either the cellular propensity to dynamic exploration could diminish as SCs mature, or, alternatively, the dynamism of adult SCs could be suppressed by external influences. One plausible mechanism would be competition for available perisynaptic space, as SCs consolidate their territory during segregation. To test this hypothesis, we acutely ablated single SCs using a two-photon femtosecond-pulsed laser (Figs. 4 and 5 and Videos 3–6; Galbraith and Terasaki, 2003; Williams et al., 2010). By parking the high-intensity laser beam briefly inside a cell's nucleus, we could ablate single SCs, as confirmed by ethidium homodimer (EtHD) influx (see Materials and methods; Fig. 4; Reddy et al., 2003). Targeted SCs quickly fragmented, vacating their original territory. Notably, nearby SCs that were bleached by exposure to a conventional continuous-wave laser for single-cell bleaching showed no evidence of phototoxicity (Fig. 4 and Video 3). Within minutes after the demise of the ablated cells, neighboring terminal SCs started to invade the newly vacated territory. Over the course of up to 5 h, the expanding cells engulfed the remnants of the ablated cell and covered the available space (n = 9/10 cases, six triangularis sterni explants; Figs. 4 B, 5 [A–C], and S4 and Video 4). Similarly, when the axonal SC next to an NMJ was ablated, terminal SCs swiftly overgrew the heminode to wrap the denuded axon (n = 5/5 cases, five triangularis sterni explants; Figs. 5 [D–F] and S4 and Video 5). In contrast, axonal SCs that adjoined an NMJ did not invade the synapse after ablation of terminal SCs over the same time period (n = 7/7 cases, four triangularis sterni explants; Figs. 5 [G–I] and S4 and Video 6). Hence, the lack of adult SC dynamism might be a result of spatial competition, in which neighboring

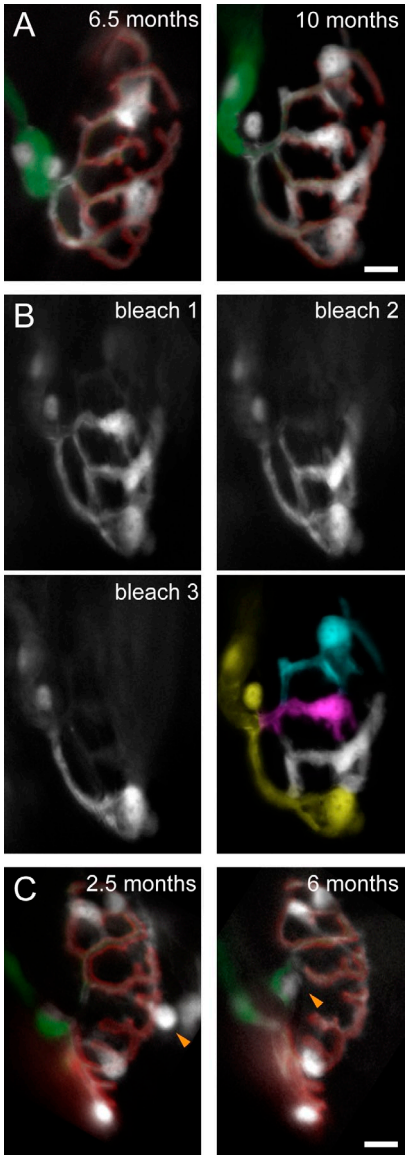

Figure 3. **Chronic in vivo imaging of mature terminal SCs.** (A and B) In vivo images of the same NMJs in the sternomastoid muscle of living SC-GFP mice obtained several weeks apart (interval 2.2 ± 1.0 mo; age at onset of imaging: 4.7 ± 1.1 mo, *n* = 53 adult NMJs, 10 mice). AChRs were labeled with a nonblocking concentration of BTX (red). Axons are labeled with *thy1*-CFP (green). (A) Addition of terminal SCs. NMJ with two terminal SCs at 6.5 mo and four terminal SCs at 10 mo. (B) Territory reconstruction of individual terminal SCs from A based on photobleaching in the living animal (bleach 1–3) reveals two new terminal SCs with substantial synaptic territory. (C) Translocation of terminal SCs. NMJ at 2.5 mo with five terminal SCs, one of which translocates across the synapse during the following 3.5 mo (orange arrowheads). Bars, 5 µm.

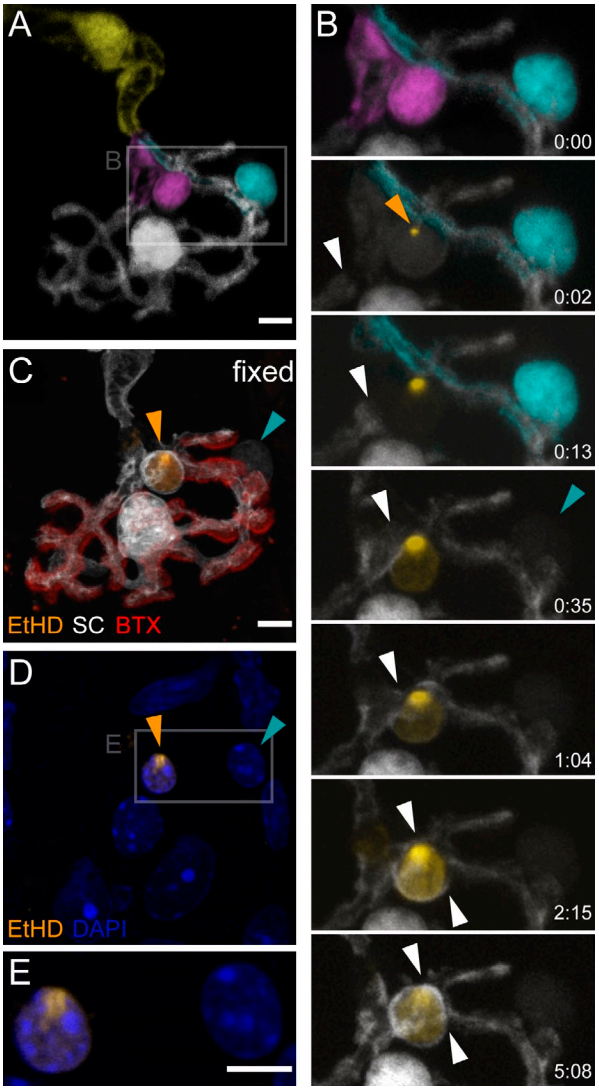

Figure 4. **Ablation of adult terminal SCs in the presence of EtHD.** (A) A pseudocolored adult NMJ with three terminal SCs (white, magenta, and cyan). (B) Time-lapse recording of area boxed in A over a period of 5 h showing a two-photon laser–induced ablation of the magenta-colored terminal SC in the presence of EtHD (orange arrowhead indicates the site of EtHD influx). After ablation of the magenta SC, the cyan cell was photobleached (cyan arrowhead). Note the absence of EtHD influx in the bleached terminal SC and the expansion (white arrowheads) of the unbleached (white) terminal SC. (C and D) Confocal view of the same NMJ after fixation and counterstaining with BTX (C) and DAPI (D). The nucleus of the ablated terminal SC is filled with EtHD (orange arrowheads in C and D), whereas the bleached terminal SC is not (cyan arrowheads in C and D). (E) Higher magnification of boxed area in D. The timers shown represent hours/minutes. Bars, 5 µm.

cells constantly push against each other without substantial changes in synaptic area they cover. However, axonal SCs seem to be constrained by additional factors at the heminode or by their state of differentiation.

SC segregation is axon dependent

Although SCs laterally abut other SCs, they are also in contact with the underlying axon terminal (Hall and Sanes, 1993). Hence, SCs could be similarly space restrained by axons, predicting that removal of axons would allow for SC dynamism and intermingling. Indeed, previous studies have demonstrated that in chronic stages after axotomy, SCs form long processes outside of NMJs, which serve as bridges to guide regeneration (Reynolds and Woolf, 1992; Kang et al., 2003). To explore whether such remodeling is accompanied by glial intermingling and dynamism, we performed single-cell labeling experiments at various times after transection of motor axons. Transection of motor nerves leads to axonal fragmentation of axons by Wallerian degeneration after a lag phase of ∼12–14 h (Coleman and Freeman, 2010). SCs remained unchanged during the lag period, suggesting that

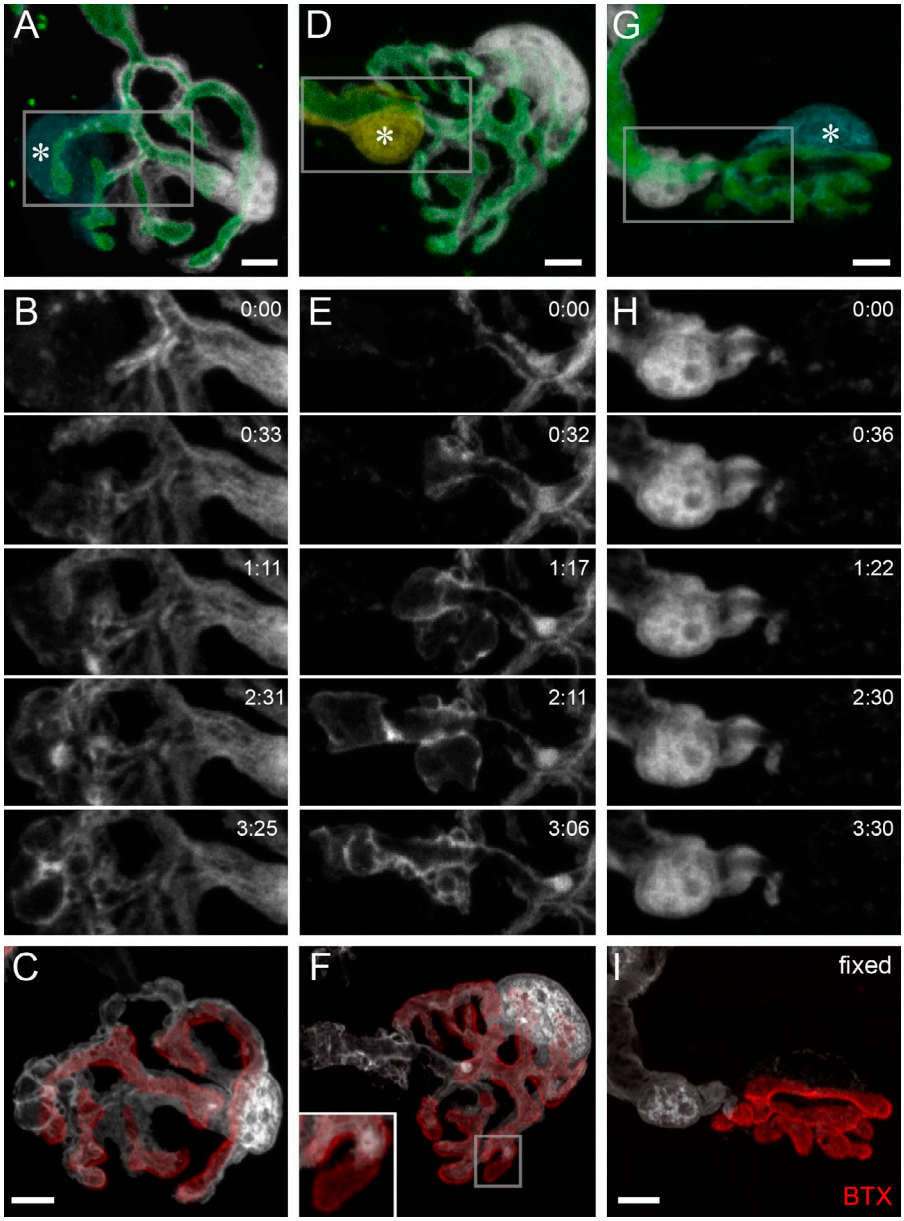

Figure 5. **Terminal SC territories are constrained by neighboring SCs at adult NMJs.** (A–C) Two-photon laser–induced ablation (A) of a terminal SC (cyan; asterisk) followed by time-lapse visualization (B) of a neighboring intact terminal SC (white) of the boxed area in A. (C) Post hoc confocal analysis after BTX (red) labeling shows complete coverage of vacated territory by the remaining terminal SC. The axon (labeled by *thy1*-Membow; green in A) remained intact (not depicted; Video 4). (D–F) Ablation (D) of axonal SC (yellow; asterisk) and time-lapse recording (E) of terminal SC (white). Confocal analysis (F) shows expansion of terminal SC along the axon (labeled by *thy1*-Membow; green in D; red [BTX] in F). (F, inset) Small postsynaptic area that was vacated during expansion (higher magnification view of boxed area). (G–I). Ablation (G) of terminal SC (cyan; asterisk) and time-lapse recording (H) of adjacent axonal SC. No takeover of territory or phagocytic activity was observed, as confirmed by confocal analysis after fixation (I; axon shown in green in G, labeled by *thy1*-OFP3; BTX in I). The timers shown represent hours/minutes. Bars, 5 µm.

solely transecting the axon was not sufficient to induce glial dynamism. The picture changed as soon as fragmentation set in. At this point, SCs engulfed and digested axonal fragments (Fig. S5). 1 d after axotomy (>24 h), single-cell labeling using photobleaching revealed evidence of intrasynaptic growth. For example, Fig. 6 (A–D) shows an NMJ 1 d after axotomy, which looks normal when all cells are labeled but reveals glial intermingling after single-cell labeling. Early formed processes stayed exclusively within the synaptic gutter or grew toward the axonal SC at the former axonal entry point (Fig. 6 [C and D] and Video 7). Quantification confirmed that SCs on denervated NMJs screened significantly more territory compared with control adult SCs (Fig. S4). At later time points (>48 h), SC growth and intermingling continued, so that the length overlap between terminal SC processes increased from a baseline of 9.0 ± 2 to 55.7 ± 4% (n = 38 pairs of SC processes each; $P < 0.001$ using a t test). Concomitantly, terminal SCs exhibit long processes inside and outside of the denervated synapse, sometimes with growth cone–like tips that rapidly extended and collapsed (Fig. 6, E–G). The SC boundary between the preterminal axon and the synapse proper was disrupted, with axonal SCs projecting processes into NMJs (n = 7/7 axonal SC) and terminal SCs projecting back into the SC tube (n = 29/78 terminal SCs). After reinnervation, segregated SC territories are reestablished, as 1 mo after denervation, SC processes recovered normal length (control: 13.9 ± 0.8 µm, n = 27 SCs; denervation: 27.3 ± 2.1 µm, n = 28 SCs; reinnervation: 12.3 ± 0.6 µm, n = 29 SCs) and overlap (reinnervation: 8.8 ± 2%, n = 38 pairs of SC processes; $P > 0.9$ between control and reinnervation using a t test).

Hence, not only neighboring SCs but also the underlying axon might suppress SC intermingling at mature NMJs. However, as Wallerian degeneration sets in with a delay, the evidence is less direct than in the case of acute laser ablation of a neighboring SC. Therefore, we sought to acutely remove axon terminals by inducing acute axonal degeneration (AAD), which fragments axon segments around a transection site within 30 min

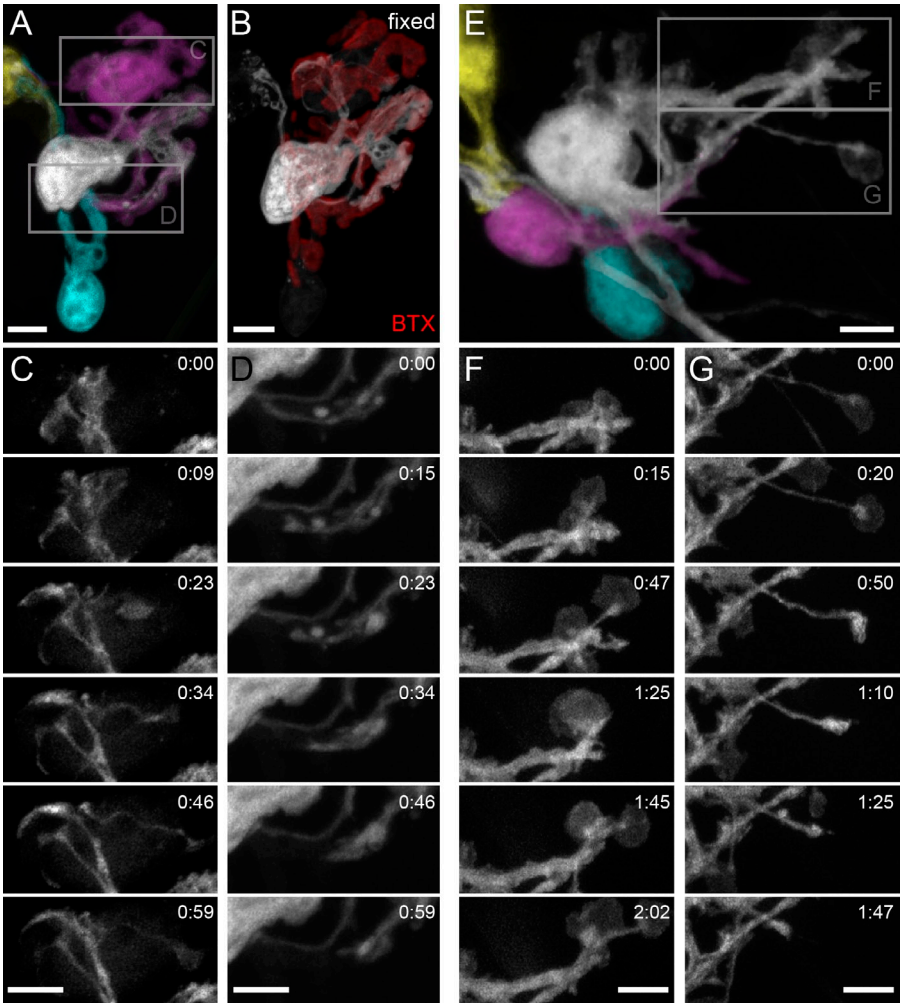

Figure 6. **SC segregation is axon dependent.** (A–D) Single-cell labeling of an NMJ 31 h after transection of the intercostal nerve. (A and B) Terminal SCs overlap but remain restricted within the synaptic gutter (labeled in B with BTX). (C and D) Time-lapse recording spanning 1 h demonstrates rapid growth (C) and retraction (D) of terminal SC processes within the synaptic gutter (depicted areas boxed in A). (E–G) 5 d after nerve transection, terminal SCs have started to sprout beyond the synapse. (F and G) Terminal SCs exhibit extrasynaptic growth cone–like structures, which grow (F) and collapse (G) rapidly over a period of 1–2 h (depicted areas boxed in E). The timers shown represent hours/minutes. Bars, 5 µm.

(Kerschensteiner et al., 2005). We transected single motor axons one node of Ranvier proximal of the final heminode using a two-photon laser (see Materials and methods; Galbraith and Terasaki, 2003; Turney and Lichtman, 2008). We then labeled single terminal SCs by sequential bleaching. As soon as fragmentation set in, terminal SCs appeared to engulf the resulting axonal debris. Soon after this (<4–5 h after laser axotomy), we observed the first outgrowth of small filopodial-like SC processes that invaded the neighboring territory (Fig. 7). Although this response appeared less dramatic than the response seen after SC ablation, careful inspection of image stacks of laser-axotomized NMJs still revealed fast volume expansion of SCs. As expected from the removal of axon terminals, which underlie all synaptic SCs, this expansion mostly occurred in the z direction along the optical axis of observation (unpublished data). Collectively, these data suggest that after axon removal, terminal SCs first expand into the vacated gutter and then start sending out processes to explore surrounding territory.

SC segregation is independent of activity but requires axonal presence

Axotomy not only leads to vacation of synaptic territory but also to loss of electrical activity, neurotransmission, and axonal transport. Chronic blockade of some of these processes is known to result in SC sprouting, even in the absence of denervation or SC loss (Son and Thompson, 1995a). Hence, we asked whether axons maintain glial segregation by their mere presence or via neural activity. To address this question, we blocked evoked neurotransmitter release in the sternomastoid muscle using botulinum toxin A (BoTX A; Rossetto et al., 2004) and used ΔNLS mice in which fragmentation is delayed after axotomy by expression of a variant of the Wallerian degeneration slow fusion protein (Beirowski et al., 2009).

When neurotransmission was blocked, even if this blockade lasted for at least 24 h (and up to 3 d), no changes in morphological parameters of SCs were apparent (Fig. 8 A), including number, length, and overlap of terminal SC processes, which remained unchanged (BoTX: 4.7 ± 0.5 processes/cell, 14.1 ± 1.2 µm/process, 8.2 ± 2.3% overlap, n = 15 SCs vs. control: 4.4 ± 0.3 processes/cell, 13.9 ± 0.8 µm/process, 7.9 ± 2.0% overlap, n = 27 SCs; $P > 0.6$ for all using a t test).

ΔNLS mice revealed that axonal fragmentation appears to be the critical factor allowing SC intermingling. As long as transected axons were preserved, no SC outgrowth or dynamism was detected (Fig. 8, B–E), even though other evidence of axotomy became apparent, such as a widening of nodes of Ranvier and variations of axonal caliber (Fig. 8 D). 1 wk after axotomy, however, when axons finally disintegrated in ΔNLS

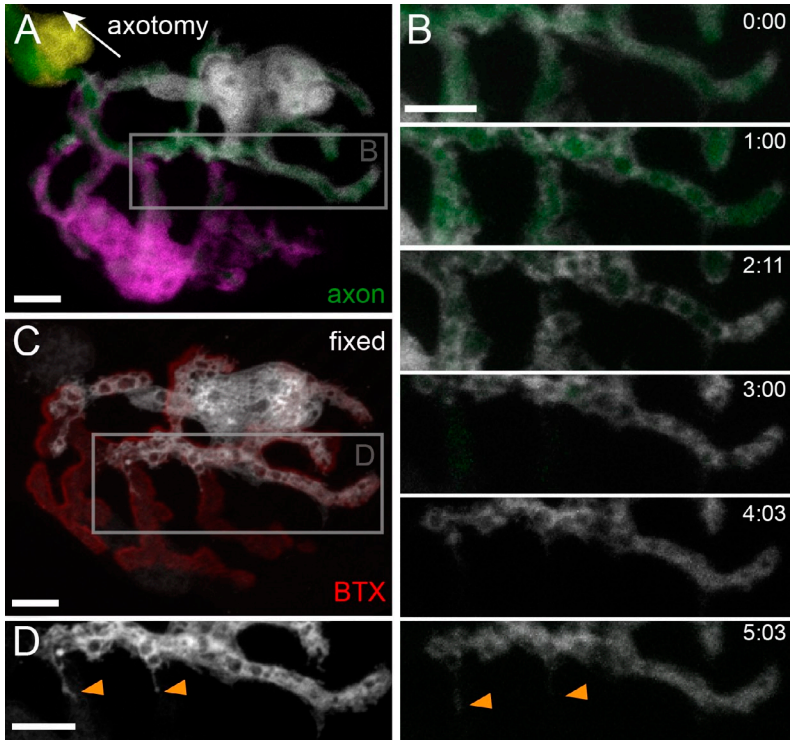

Figure 7. **Acute axon removal causes delayed SC expansion.** (A) NMJ with single-cell labeling before two-photon laser–induced axonal degeneration (SCs pseudocolored in white, magenta, and yellow). The axon was severed at the second node of Ranvier away from the synapse (white arrow indicating direction; not in frame). (B) Time-lapse recording over a period of 5 h shows AAD (note fragmentation after 1 h), which led to local SC outgrowth (orange arrowheads; shown in area boxed in A). (C and D) Fixation after 5 h and staining for BTX reveal local outgrowth along several NMJ branches (orange arrowheads in D show fixed SC channel only in the area boxed in C). The timers shown represent hours/minutes. Bars, 5 µm.

mice, SCs started to expand, indicating that the transgene does not induce a general defect in the ability of SCs to grow (unpublished data). Together, these results rule out neuronal activity and axonally transported mediators as the cues that hold adult SCs in place, which is compatible with a space constraint hypothesis of glial segregation.

Discussion

Here, we analyze the cellular mechanisms that constrain glial cells at a mammalian model synapse, the NMJ. Using newly developed tools to label and ablate single SCs, as well as optical, pharmacological, and genetic manipulations, we reveal that mature SCs statically tile the synapse. This arrangement emerges during development from a dynamic shingling pattern, in which SCs constantly explore territory within and beyond the synaptic site. Laser ablation experiments reveal that the adult tiling pattern is maintained by glial–glial and axonal–glial interactions, compatible with a competition for perisynaptic space.

The tools of conventional labeling and microscopy are insufficient to reveal the precise relationship between glial cells and synapses (Bushong et al., 2002), even at a synapse as simple as the NMJ. For example, the borders between individual terminal SCs cannot be resolved by light microscopy, as terminal SC membranes are in direct apposition, as revealed by EM (Desaki and Uehara, 1981). Here, we devise two strategies to circumvent this problem: sequential filling and photobleaching, both of which have been used successfully to delineate glial cells in the central nervous system (CNS; Bushong et al., 2002; Williams et al., 2010). Both approaches yield complementary results (compare Fig. 1 and Fig. S1) and compensate for the other's shortcomings. For example, sequential filling requires intracellular access and can involve destruction of labeled cells after documentation; hence, it is not suitable for studying the dynamics of single cells. Sequential bleaching, on the other hand, allows for labeling of untouched single cells that can be followed over time; however, only the last unbleached cell can be revealed in a positive image. The outlines of all other cells, obtained by image subtraction, are prone to noise, which adds uncertainty to fine detail. In addition, bleaching could induce phototoxicity, which might alter SC morphology or dynamism. However, several lines of argument (see Materials and methods), including the matching results obtained by filling and bleaching, argue against significant phototoxic effects in our study.

For mature NMJs, our labeling approach revealed that terminal SCs are constrained to within the perisynaptic space both along the muscle surface as well as at the entry point of the innervating axon and that within the perisynaptic space, terminal SCs establish nonoverlapping domains.

Which factors might contribute to retaining SCs within the perisynaptic space? The basal lamina at the NMJ fills the synaptic cleft, but also surrounds SCs and muscle fibers, to form a pouch around axon terminals and terminal SCs. Thus, the basal lamina and molecular cues contained within seem like probable candidates to laterally constrain SCs. Indeed, deletion of synaptic laminin-β2 (Noakes et al., 1995; Patton et al., 1998) allows invasion of terminal SC processes around axon terminals into the synaptic cleft; such SC fingers are present at amphibian NMJs. Amphibian NMJs show dynamic remodeling even in the adult, a process accompanied by basal lamina expansion, supporting the notion of an ECM constraint (Chen and Ko, 1994). The basal lamina pouch surrounding NMJs contains at least one discontinuity, though: the synaptic entry point where the motor axon enters. Here, the last axonal SC forms a

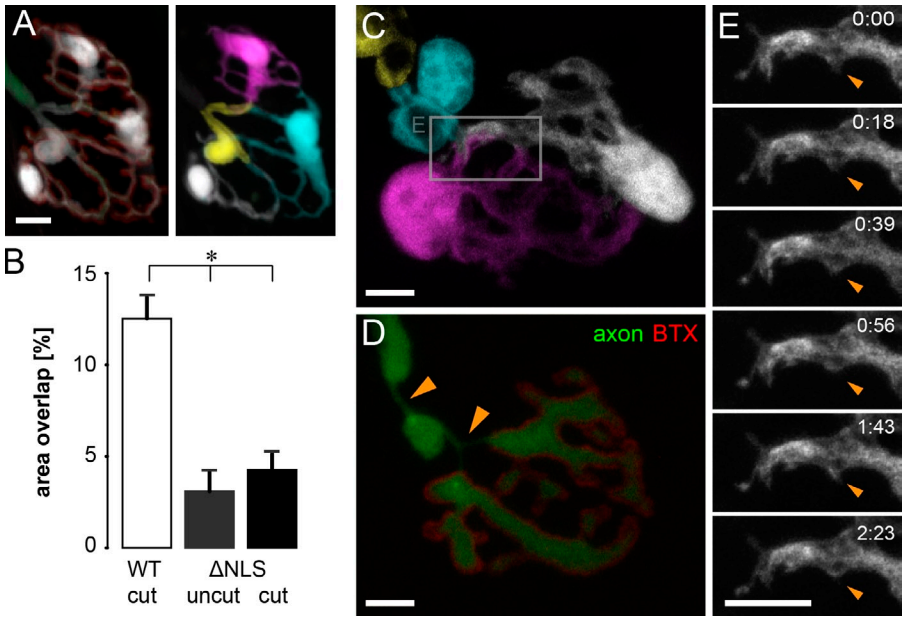

Figure 8. **SC segregation is activity independent but requires axonal presence.** (A) Block of neurotransmission by BoTX treatment did not alter morphology of SCs after 3–4 d. Axon (green), synaptic gutter (BTX [red]) and SCs (white [left] and individually pseudocolored [right]). (B–E) Mice with delayed axon fragmentation (ΔNLS) do not show SC intermingling for up to 2 d after transection. (B) Quantification of area overlap after axotomy in ΔNLS mice (mean of SCs + SEM; *, $P < 0.01$ using a *t* test; ΔNLS cut, $n = 36$ SC pairs, three triangularis sterni muscles; ΔNLS uncut, $n = 20$ SC pairs, three triangularis sterni muscles; WT cut, $n = 31$ SC pairs, seven triangularis sterni muscles). (C) Single-cell labeling of an NMJ 2 d after axotomy shows segregated SCs and a preserved axon (D) on top of the synaptic gutter (BTX). Despite preserved axon continuity, local axon atrophy was observed (orange arrowheads in D). (E) Time-lapse microscopy over a period of >2 h demonstrates the lack of terminal SC dynamism at axotomized ΔNLS NMJs (shown in the area boxed in C). The timers shown represent hours/minutes. Bars, 5 µm.

heminode and engages in tight paranodal adhesions with the axon. This barrier likely constrains terminal SCs by preventing retrograde growth along the axon. Indeed, our ablation experiments reveal that terminal SCs expand along the axon as soon as the last axonal SC is removed. However, if terminal SCs are ablated, axonal SCs are still incapable of invading the synapse. Previous experiments using global destruction of perisynaptic glial cells at frog NMJs also showed little acute changes in the morphology of the surviving axonal glia (Reddy et al., 2003). In contrast, genetic deletions of the paranodal adhesion induce spontaneous SC invasion into the nodal domain (Thaxton et al., 2011).

However, neither basal lamina constraints nor axon–glial adhesions are likely candidates to constrain individual terminal SCs within the space delineated by the ECM. Little, if any, basal lamina is present between terminal SCs or between terminal SCs and axons (Hall and Sanes, 1993). Instead, glial–glial interactions likely underlie synaptic partitioning. Ablation of single terminal SCs supported this idea, as surviving terminal SCs immediately invaded the liberated space. Two possible models of glial–glial interaction can explain this result: on the one hand, homotypic repulsion, as has been discussed for axon and dendrite branches (Sagasti et al., 2005) but also for CNS glial processes (Nimmerjahn et al., 2005; Kirby et al., 2006), and on the other hand, an opportunistic space filling model, in which each terminal SC attempts to occupy as much space as possible within the confines of the outer basal lamina pouch.

Although our data do not exclude homotypic repulsion, the results are more suggestive of a space filling model for several reasons: First, our time-lapse observations of individual mature SCs show little evidence of continuous expansion and retraction that is characteristically observed in the case of contact-mediated repulsion. Rather than repulsing each other, terminal SCs appear to be in permanent contact. Second, removal of axon terminals, either by Wallerian or AAD, also induced SC expansion, suggesting that homotypic interactions are at least not the sole constraint. Third, immature terminal SCs readily intermingle, providing little evidence for homotypic repulsive cues.

Assuming that limited perisynaptic space constrains mature terminal SCs, how can we explain the exploratory behavior of immature SCs? One obvious difference between mature and immature NMJs lies in the highly dynamic nature of immature axon terminals themselves. First, during this period, a large number of axon terminals gets eliminated from the synapse, liberating space within the synapse (Sanes and Lichtman, 1999). Second, axon terminals from different motor axons are sorted into segregated domains (Gan and Lichtman, 1998), which could require some compensatory glial dynamism, even if individual SCs are not assigned to individual axonal inputs (Fig. S2). Third, even at singly innervated young NMJs, axon terminals swiftly grow and retract small processes (Walsh and Lichtman, 2003), suggesting a much looser arrangement of cells at the synapse. Finally, the basal lamina develops only gradually during the postnatal period with those parts surrounding SCs emerging late (Hall and Sanes, 1993), allowing immature SCs, as well as axons, to send processes beyond synaptic boundaries. The emergence of strictly segregated glial domains, in this view, results from progressive filling up of perisynaptic space as the synapse stabilizes. Subsequent pruning then removes intermingled processes that remain after dynamism ceases, very much like pruning removes exuberant glial processes during establishment of astrocytic domains (Bushong et al., 2003).

Although our observations of glial expansion after axon removal are compatible with a space competition model, additional influences could obviously modulate glial behavior, including loss of neuronal activity, loss of modulators delivered by axonal transport, and factors released during cellular fragmentation or phagocytosis. Our findings argue that at least the first two mechanisms do not play an important role. First, directly blocking evoked neurotransmitter release with BoTX for several days did not cause glial intermingling, even though chronic treatment with activity blockers is known to eventually cause glial outgrowth

(Son and Thompson, 1995a). Although previous experiments (Brown et al., 1981; Kang et al., 2003) show that a single topical application of BoTX suffices to block release for several days, we cannot exclude a partial return of release toward the end of the 3–4-d period we assayed or of some transmitter leakage throughout. However, our results do support the conclusion that outgrowth of terminal SC within 1 d after axotomy is not caused by loss of release, given that in our BoTX experiments, blockade was probably complete for at least >1 d, and spontaneous release should have persisted after axotomy until fragmentation sets in. Second, genetically delaying axon fragmentation also delayed glial intermingling, arguing that neither neuronal activity (transmitter release or action potential propagation) nor fast axonal transport (which ceases after axotomy within 1 d; Misgeld et al., 2007) directly impacts the glial response. We cannot fully exclude the third possibility, namely that glial expansion was also modulated by factors released during cell ablation. However, the observation that only those SCs that abutted ablated cells expanded their territory and that such expansion originated only from parts of the cell directly facing vacated sites argues against global activation by diffusible factors released during fragmentation. Instead, SC expansion in one part of the synapse was accompanied by retraction from another (Fig. 5 F, inset), suggesting that SC cytoplasm is reallocated within the cell during expansion. This implies that there might be a limit to the degree to which a single terminal SC could acutely expand. Whether more chronic ablations of terminal SCs would result in proliferation of remaining cells and what the consequences of chronic loss and expansion of terminal SCs for synaptic function would be could be addressed in future experiments using our approach (compare with Reddy et al., 2003).

To our surprise, beyond the predicted expansion, terminal SCs also showed a dramatic capacity to engulf the debris of ablated cells. SCs are known to be capable of phagocytosis, but, generally, this capacity is believed to be acquired in response to injury-induced dedifferentiation, as seen during Wallerian degeneration, when SCs participate in the removal of axon and myelin debris (Miledi and Slater, 1968; Hirata and Kawabuchi, 2002). However, our data suggest that SCs are endowed with the immediate ability to engulf nearby cellular debris. Indeed, during development, glial cells contribute to physiological clearance of axonal fragments (Awasaki and Ito, 2004; Bishop et al., 2004; Watts et al., 2004; Song et al., 2008). Thus, our study reveals hitherto unappreciated characteristics of terminal SCs, the first being their dramatic response to nearby cell ablations and their propensity to immediately engulf debris. This suggests similarities to CNS microglia (Nimmerjahn et al., 2005). Together with their developmental role as axon scavengers (Bishop et al., 2004; Song et al., 2008), this extends the aggressive potential of terminal SCs into adulthood. Second, how mature terminal SCs partition synaptic space is reminiscent of the nonoverlapping space filling arrangement of astrocytes in the mature brain (Bushong et al., 2002; Nedergaard et al., 2003; Livet et al., 2007; Reichenbach et al., 2010). Also, the developmental exuberance of terminal SCs, as well as their limited dynamism at maturity, resembles astrocytic behavior (Bushong et al., 2004; Haber et al., 2006; Reichenbach et al., 2010). Thus, terminal SCs are multifaceted glial cells that can serve as versatile models of glial function during development and in health and disease.

Materials and methods

Experimental animals

The following transgenic mice were used in our experiments: SC-GFP mice, which express GFP in SCs driven either by the *s100b* (line K; Zuo et al., 2004) or *plp* promoters (provided by W. Macklin, University of Colorado Denver Anschutz Medical Campus, Aurora, CO; Mallon et al., 2002). *s100B*-GFP mice were used for sequential SC filling, short-term denervation experiments, and BoTX treatment. Furthermore, transgenic mice expressing GFP driven by the *nestin* promoter and its neural enhancer (line F) were used in some denervation experiments (Mignone et al., 2004), as the *s100* promoter down-regulates after denervation (Kang et al., 2003). Time-lapse experiments in axotomized and in developing animals, as well as SC ablations, were performed in *plp*-GFP mice. To label axons, SC-GFP mice were crossbred with *thy1*-XFP mice, which express OFP (*thy1*-OFP, line 3), membrane-RFP (*thy1*-Membow, line 13; Livet et al., 2007), or CFP (*thy1*-CFP, line C) under the control of a modified *thy1* regulatory cassette (Feng et al., 2000).

Transgenic mice expressing the Wallerian degeneration slow fusion protein, which was modified by two point mutations in the Nmnat1 domain to redistribute the gene product from the nucleus to the cytoplasm (ΔNLS mice), were crossed with *plp*-GFP and *thy1*-OFP mice to monitor how SC dynamics change when axonal fragmentation is delayed after axotomy (Beirowski et al., 2009; mice were provided by M. Coleman, Babraham Institute, Cambridge, England, UK). Animal procedures were approved by the Animal Study Committee of the Regierung von Oberbayern, the Institutional Animal Care and Use Committee of the University of Texas at Austin, and the Institutional Animal Care and Use Committee of the University of California, Santa Cruz.

Photobleaching of individual SCs and axons

Adult mice (>7 wk of age, both sexes) were anesthetized using isoflurane, and nerve–muscle explants, including the triangularis sterni (McArdle et al., 1981), were isolated as previously described (Kerschensteiner et al., 2008). In brief, mice were killed using isoflurane and were sprayed with 70% ethanol. A midline incision of the skin over the sternum and two incisions parallel to the lower borders of the rib cage were made to remove the skin and the pectoral muscles. The diaphragm was cut, followed by cutting the ribs along the vertebral column. The explanted thorax was transferred into a dish with oxygenated precooled Ringer's solution (125 mM NaCl, 2.5 mM KCl, 1.25 mM NaH_2PO_4, 26 mM $NaHCO_3$, 2 mM $CaCl_2$, 1 mM $MgCl_2$, and 20 mM glucose), and remnants of thymus, pleura, and muscles were removed. The cleaned thorax (nerve–muscle explant) was pinned onto a Sylgard-coated dish, superfused with oxygenated Ringer's solution, and heated to 32–35°C during imaging.

For photobleaching of individual SCs, we used a confocal microscope (FV1000; Olympus) equipped with water immersion objectives (100x, 1.0 NA and 60x, 0.9 NA) and an argon laser. The 488-nm laser beam was centered on the nucleus of an SC, and the tornado scan function was used to bleach GFP at maximum power for 5 s followed by a short break. If necessary, this procedure was repeated until GFP levels were reduced to near-background levels. This procedure was repeated for all but one cell. Subtractive labeling depends on the fact that the majority of GFP molecules diffuse through the hourglass-shaped profile of a laser beam, which can be constrained to within an SC nucleus. As SC nuclei at the NMJ are often slightly displaced from the synapse itself, single SCs can be bleached in their entirety without collateral bleaching of their neighbors. We acquired confocal images after every bleach step and subtracted the resulting images to delineate single SC territories.

Thy1-OFP–labeled axons were bleached as described above using a 559-nm solid-state laser. The laser beam was placed into one of several axons entering a developing NMJ. Bleaching intervals lasted at least 10 s. Confocal images were acquired as fast as possible to avoid refilling of the NMJ by diffusion from the large pool of fluorescent protein in distant parts of the axon. Image subtraction revealed the synaptic territory occupied by individual axons (Turney and Lichtman, 2008). To visualize synaptic sites, we used bungarotoxin (BTX) coupled to Alexa Fluor 647 (Invitrogen) at a concentration of 0.8 µg/ml and applied for 15–20 min at room temperature in oxygenated Ringer's solution.

The following points argue against phototoxic effects as a result of the bleaching procedure as major contributors to the cellular behavior we observed: bleaching of an SC did not induce any morphological alterations in nearby axons, SCs, or underlying muscle fibers (specifically, contraction clots, which are the common indicator of phototoxic damage in muscle, were not observed; van Mier and Lichtman, 1994); over several hours after bleaching, the total area of nonablated SCs did not change, despite substantial dynamism at least in young SCs (Fig. 2, I and J), which is very much in contrast to SCs whose neighbors were deliberately killed (see SC ablation and EtHD application; Fig. 5); bleached (but not ablated) SCs excluded EtHD (see SC ablation and EtHD application; Fig. 4); and, finally, the correspondence of data obtained by subtractive and additive labeling (see next section) supports the notion that bleaching does not alter the morphology of SCs in our experiments.

Dye filling

Young adult animals (2–4 mo of age, both sexes) were killed with an overdose of ketamine/xylazine and were perfused with oxygenated Ringer's solution. We dissected the sternomastoid muscle, pinned it at resting length into a Sylgard-coated dish, superfused it with oxygenated Ringer's solution, and stained the muscle with Alexa Fluor 594– or rhodamine-coupled BTX (Invitrogen). NMJs near the center of the muscle fibers were observed with water immersion objectives (40x, 0.75 NA and 63x, 0.90 NA; Carl Zeiss) on a wide-field microscope (Axiotech; Carl Zeiss). A double band filter set (Chroma Technology Corp.) was used to simultaneously view both rhodamine and GFP fluorescence. NMJs at the muscle surface with an en face orientation were selected for injection. We pulled thin-tipped microelectrodes from borosilicate glass capillaries with a filament (1B120F-4; World Precision Instruments); such electrodes had a resistance of 60 MΩ after backfilling them with a solution containing 2% rhodamine dextran in 3 M K acetate (1% neurobiotin was included in addition during experiments aimed at detecting SC coupling). After penetrating the membrane, two to five quick depolarizing pulses (~1 nA) were used to iontophorese dye into SCs. After dye filling, the electrode was removed, and the different fluorochromes were imaged separately with appropriate filter sets (Chroma Technology Corp.). To label further cells, the initially labeled cell was destroyed by disrupting its membrane with the microelectrode, and the next cell was filled as previously described. Images were collected with a charge-coupled device camera (Princeton MicroMAX; Roper Scientific) controlled by IPLab software (Scanalytics, Inc.).

Repetitive in vivo imaging

We imaged NMJs in living 2–4-mo-old mice using the method developed by Lichtman et al. (1987). In brief, each animal was anesthetized with ketamine/xylazine (0.10–0.15 ml of 0.9% NaCl solution containing 17.4 mg/ml ketamine and 2.6 mg/ml xylazine). We performed a ventral midline incision in the neck to expose the sternomastoid muscle. Acetylcholine receptors (AChRs) were labeled by application of Alexa Fluor 594– or rhodamine-conjugated BTX (5 µg/ml) in sterile lactated Ringer's solution applied for 5 min. The animal was intubated endotracheally, and its respiration was driven by a small rodent respirator (Harvard Apparatus). A number 0 coverslip held orthogonal to the optical axis of the microscope was applied to the muscle surface to slightly depress and flatten it during imaging to minimize movement artifacts. Images were collected using the same wide-field system described in the previous section. After imaging, the incision was closed with 6–0 silk suture, and the animal was allowed to recover from anesthesia under a heat lamp and was then returned to its cage. In individual cases, single-cell bleaching was performed in vivo at the last imaging time point.

SC ablation and EtHD application

We ablated SCs in nerve–muscle explants of *plp*-GFP × *thy1*-OFP mice using a multiphoton microscopy system (FV1000) equipped with a femtosecond-pulsed titanium sapphire laser (MaiTai; Newport Corporation) and a set of continuous-wave lasers for confocal image acquisition. Before ablation, we obtained a confocal image of the selected NMJ. Then, the MaiTai laser beam (tuned to 840 nm) was placed inside an SC nucleus, and a small circular region of interest was exposed using the tornado scan function (10–30 frames and 10–30% of a maximum of ~100–300 mW in the back-focal plane). If the first pulse did not kill the SC (judged by the formation of cellular fragments), a second pulse with increased power was applied. To avoid axonal damage, we took care to only select SCs with nuclei that did not overlie axons. To observe a single nonablated SC nearby, all other remaining SCs were bleached as previously described. To directly verify that cells were killed by this procedure (and that others remain viable after the bleaching procedure), we added EtHD (Invitrogen) to the oxygenated Ringer's solution at a concentration of 0.5 µg/ml (Reddy et al., 2003).

Denervation surgery and laser axotomy

Standard procedures were used to denervate the triangularis sterni (McArdle et al., 1981) and sternomastoid muscles (Rich and Lichtman, 1989). In brief, anesthetized animals were placed in the supine position on a magnetic stainless steel plate with the limbs and upper jaw secured with rubber bands attached to magnets. For denervating parts of the triangularis sterni muscle, we performed a lateral incision through the skin overlying the ribs, exposed the intercostal nerve in the second or third intercostal space, and transected the nerve using fine iridectomy scissors. For the sternomastoid muscle, a ventral midline incision in the neck was used to expose the muscle. The nerve to the left sternomastoid muscle was axotomized or crushed ~6 mm away from the muscle. We closed the surgical opening as previously described and returned the animal to its cage for recovery.

We used laser axotomy to induce AAD (Kerschensteiner et al., 2008) in triangularis sterni explants of *plp*-GFP mice crossed to *thy1*-XFP mice to covisualize axons. Single motor axons were transected using a procedure similar to SC ablation as described in the previous section. Instead of a tornado scan, we used a linescan (80–100% laser power at 910 nm) across a node of Ranvier, which was separated from the NMJ by at least two SCs (to avoid damage to any SC directly abutting the NMJ under study). Confocal images were taken before and after the induction of AAD. If no sign of axonal fragmentation was observed within 30 min, a second linescan was applied. This generally allowed axotomy without damage to SCs or muscle fibers that were part of the NMJ under study.

BoTX administration

We exposed the left sternomastoid muscle as described in Repetitive in vivo imaging. BoTX A (0.2 ng in 20 µl of 0.1 M PBS with 0.2% gelatin; EMD) was applied directly to the muscle surface for 5 min. Drug solution was washed away several times with Ringer's solution, and the skin was sutured after removal of excess fluid. The same procedure was used for control animals, except that only vehicle (20 µl of 0.1 M PBS with 0.2% gelatin) was applied. At the time the muscles were removed, they were examined for contraction elicited by nerve stimulation. Muscles remained completely paralyzed for 3 d after a single application of BoTX. 7 d after application, nerve-evoked muscle twitch and tetanic tensions were 2–6% of tensions elicited by direct muscle stimulation.

Staining and imaging of fixed muscles

Muscles were fixed with 4% PFA in PBS for 30–60 min after imaging. We washed the muscles and incubated them with 3 µg/ml Cy5-streptavidin in 2% Triton X-100 in PBS (to detect neurobiotin) or Cy5- or Alexa Fluor 647–coupled BTX (3 µg/ml to label postsynaptic AChRs) for 2 h. The anti-Caspr antibody (a gift from E. Peles, Weizmann Institute of Science, Rehovot, Israel; Peles et al., 1997) was used at a concentration of 1:800 in 0.2% Triton X-100 and 1% BSA in PBS followed by incubation with appropriate secondary antibodies in PBS. Entire triangularis sterni muscles and thin layers dissected from sternomastoid muscles were mounted in fluorescence mounting media and examined using either wide-field or confocal microscopy.

Data quantification

For quantitative analysis, we used Fiji (a package based on the open-source software ImageJ; National Institutes of Health) or IPLab software.

Overlap and segregation of SCs

To quantify the degree of overlap between SCs, we used two methods. First, we measured the length of terminal SC processes of single cells and, in merged images, determined the overlap between the processes of pairs of cells (length overlap). Second, using NMJs with two terminal SCs, we generated binarized images (Li auto-thresholding algorithm; Fiji) of the two SCs and the NMJ (as outlined by BTX). Area overlap was quantified as the ratio between the number of pixels occupied by both SCs and the overall number of NMJ pixels (overlap area over total NMJ area).

To quantify the degree of segregation of SCs (i.e., the degree to which their territories occupy distinct parts of the synapse; Gan and Lichtman, 1998), we used the same binarization approach as detailed above. The binarized BTX image of the NMJ was used as a mask and was superimposed on the SC images. Then, we determined the location of the centroid of fluorescence of each SC. Segregation was expressed as the ratio of the distance of the two centroids over the width of the NMJ

measured through the centroids (because of masking and the fact that two cells cannot occupy the same space, this value does not span the range from 0–100%; instead, we found extreme values as low as 8% and as high as 54%).

Territory exploration over time

Time-lapse videos over a period of 1 h (time interval of ∼10 min) of single SCs were converted to binary versions using the auto-threshold Li algorithm as described in the previous section. We measured the mean SC area and the area of the maximum intensity projection of all frames. The explored territory was calculated by first subtracting the mean territory from the maximum territory (i.e., determining the part of the territory an SC temporarily explored but did not maintain for most of the time) and by then normalizing this difference to the mean territory (to account for differences in SC sizes).

Image representation

Confocal image stacks and wide-field images were assembled for representation using Photoshop software (Adobe). Maximum intensity projections were generated using Fiji; alternatively, in-focus parts of NMJs were manually extracted from multiple focal planes in Photoshop. To generate multicolor representations of individually labeled SCs, we used image subtraction (in the case of sequential bleaching) and manual isolation (for filling) to define the territories of single SCs. Isolated structures, likely artifacts as a result of noise or labeled debris, were not included if inspection of the image stacks did not provide evidence for cellular continuity with the labeled SC. Then, colored representations were superimposed as semi-opaque objects on projected views of the NMJs before single-cell labeling. For better visibility of dim structures, γ was adjusted.

Statistics

The number of objects (n) counted in individual experiments is indicated in the text or figure legends. Error bars are presented as value + SEM (based on the number of objects). Comparisons between two groups were performed with unpaired t tests. Differences between groups were considered significant when $P < 0.05$. Asterisks indicate $P < 0.01$.

Online supplemental material

Fig. S1 shows that terminal SCs form a distinct compartment from axonal SCs using sequential dye filling, Caspr immunohistochemistry, and dye-coupling experiments. Fig. S2 illustrates that young terminal SCs are not assigned to single axonal inputs. Fig. S3 demonstrates that young, immature axonal SCs explore synaptic territory, whereas adult axonal SCs are static. Fig. S4 displays a summary graph of explored territory by SCs in young and adult NMJs as well as after axotomy or SC ablation. Fig. S5 shows engulfment of axonal fragments by SCs 12 h after axotomy. Video 1 shows dynamism of young SCs isolated by photobleaching of neighboring SCs and visualized by time-lapse confocal microscopy over a period of 2 h and 21 min. Video 2 illustrates the static nature of adult SCs after photobleaching of abutting SCs using time-lapse confocal microscopy over a period of 3 h and 8 min. Video 3 shows an adult NMJ with three terminal SCs; one terminal SC was laser ablated, the second one was bleached, and the third one was followed by time-lapse confocal microscopy over a period of 5 h and 29 min in the presence of the nuclear dye EtHD. Video 4 shows ablation of a terminal SC and expansion of its neighbor in an adult NMJ in a confocal time lapse over 3 h and 25 min. Video 5 shows ablation of an adult axonal SC leading to internodal expansion of a terminal SC, as visualized by time-lapse confocal microscopy over a period of 3 h and 26 min. Video 6 illustrates ablation of an adult terminal SC that did not result in expansion of the neighboring axonal SCs, as assayed by time-lapse confocal microscopy over a period of 3 h and 30 min. Video 7 shows an adult NMJ 31 h after axotomy. Using time-lapse confocal microscopy and photobleaching, we followed a single terminal SC over a period of 1 h and 43 min. Online supplemental material is available at http://www.jcb.org/cgi/content/full/jcb.201108005/DC1.

We would like to thank M. Budak, K. Wullimann, Y. Hufnagel, and Lj. Marinković for excellent technical assistance and R. Karl and A. Thomer from Dr. A. Konnerth's laboratory for their kind support. We thank Drs. L. Godinho and P. Williams for critically reading the manuscript. We are grateful to Dr. W. Macklin for the generous gift of *plp*-GFP mice, to Dr. M. Coleman for ΔNLS mice, and to Dr. E. Peles for providing anti-Caspr antibodies.

T. Misgeld was supported by the Technische Universität München Institute of Advanced Studies, the Deutsche Forschungsgemeinschaft (Sonderforschungsbereich grant SFB 596), the Alexander von Humboldt Foundation, the Federal Ministry of Education and Research (European Research Area Network iPSoALS and 2-p imaging projects), and the Center for Integrated Protein Science Munich. Y. Zuo was supported by the Ellison Medical Foundation and the National Institutes on Aging. Work on this project in W. Thompson's laboratory was supported by the National Institutes of Health (grant NS020480).

Author contributions: M.S. Brill, J.W. Lichtman, T. Misgeld, W. Thompson, and Y. Zuo conceived the experiments. M.S. Brill, T. Misgeld, and Y. Zuo performed imaging experiments and evaluated data. J.W. Lichtman and W. Thompson provided mouse strains. M.S. Brill, T. Misgeld, and Y. Zuo wrote the paper.

Submitted: 1 August 2011
Accepted: 13 September 2011

References

Araque, A., V. Parpura, R.P. Sanzgiri, and P.G. Haydon. 1999. Tripartite synapses: glia, the unacknowledged partner. *Trends Neurosci.* 22:208–215. http://dx.doi.org/10.1016/S0166-2236(98)01349-6

Awasaki, T., and K. Ito. 2004. Engulfing action of glial cells is required for programmed axon pruning during *Drosophila* metamorphosis. *Curr. Biol.* 14:668–677. http://dx.doi.org/10.1016/j.cub.2004.04.001

Barres, B.A. 2008. The mystery and magic of glia: a perspective on their roles in health and disease. *Neuron*. 60:430–440. http://dx.doi.org/10.1016/j.neuron.2008.10.013

Beirowski, B., E. Babetto, J. Gilley, F. Mazzola, L. Conforti, L. Janeckova, G. Magni, R.R. Ribchester, and M.P. Coleman. 2009. Non-nuclear Wld(S) determines its neuroprotective efficacy for axons and synapses in vivo. *J. Neurosci.* 29:653–668. http://dx.doi.org/10.1523/JNEUROSCI.3814-08.2009

Birks, R., B. Katz, and R. Miledi. 1960. Physiological and structural changes at the amphibian myoneural junction, in the course of nerve degeneration. *J. Physiol.* 150:145–168.

Bishop, D.L., T. Misgeld, M.K. Walsh, W.B. Gan, and J.W. Lichtman. 2004. Axon branch removal at developing synapses by axosome shedding. *Neuron*. 44:651–661. http://dx.doi.org/10.1016/j.neuron.2004.10.026

Brown, M.C., R.L. Holland, and W.G. Hopkins. 1981. Restoration of focal multiple innervation in rat muscles by transmission block during a critical stage of development. *J. Physiol.* 318:355–364.

Bushong, E.A., M.E. Martone, Y.Z. Jones, and M.H. Ellisman. 2002. Protoplasmic astrocytes in CA1 stratum radiatum occupy separate anatomical domains. *J. Neurosci.* 22:183–192.

Bushong, E.A., M.E. Martone, and M.H. Ellisman. 2003. Examination of the relationship between astrocyte morphology and laminar boundaries in the molecular layer of adult dentate gyrus. *J. Comp. Neurol.* 462:241–251. http://dx.doi.org/10.1002/cne.10728

Bushong, E.A., M.E. Martone, and M.H. Ellisman. 2004. Maturation of astrocyte morphology and the establishment of astrocyte domains during postnatal hippocampal development. *Int. J. Dev. Neurosci.* 22:73–86. http://dx.doi.org/10.1016/j.ijdevneu.2003.12.008

Chen, L., and C.P. Ko. 1994. Extension of synaptic extracellular matrix during nerve terminal sprouting in living frog neuromuscular junctions. *J. Neurosci.* 14:796–808.

Coleman, M.P., and M.R. Freeman. 2010. Wallerian degeneration, wld(s), and nmnat. *Annu. Rev. Neurosci.* 33:245–267. http://dx.doi.org/10.1146/annurev-neuro-060909-153248

Desaki, J., and Y. Uehara. 1981. The overall morphology of neuromuscular junctions as revealed by scanning electron microscopy. *J. Neurocytol.* 10:101–110. http://dx.doi.org/10.1007/BF01181747

Eroglu, C., and B.A. Barres. 2010. Regulation of synaptic connectivity by glia. *Nature*. 468:223–231. http://dx.doi.org/10.1038/nature09612

Feng, G., R.H. Mellor, M. Bernstein, C. Keller-Peck, Q.T. Nguyen, M. Wallace, J.M. Nerbonne, J.W. Lichtman, and J.R. Sanes. 2000. Imaging neuronal subsets in transgenic mice expressing multiple spectral variants of GFP. *Neuron*. 28:41–51. http://dx.doi.org/10.1016/S0896-6273(00)00084-2

Galbraith, J.A., and M. Terasaki. 2003. Controlled damage in thick specimens by multiphoton excitation. *Mol. Biol. Cell*. 14:1808–1817. http://dx.doi.org/10.1091/mbc.E02-03-0163

Gan, W.B., and J.W. Lichtman. 1998. Synaptic segregation at the developing neuromuscular junction. *Science*. 282:1508–1511. http://dx.doi.org/10.1126/science.282.5393.1508

Haber, M., L. Zhou, and K.K. Murai. 2006. Cooperative astrocyte and dendritic spine dynamics at hippocampal excitatory synapses. *J. Neurosci.* 26:8881–8891. http://dx.doi.org/10.1523/JNEUROSCI.1302-06.2006

Hall, Z.W., and J.R. Sanes. 1993. Synaptic structure and development: the neuromuscular junction. *Cell*. 72(Suppl):99–121. http://dx.doi.org/10.1016/S0092-8674(05)80031-5

Hirata, K., and M. Kawabuchi. 2002. Myelin phagocytosis by macrophages and nonmacrophages during Wallerian degeneration. *Microsc. Res. Tech.* 57: 541–547. http://dx.doi.org/10.1002/jemt.10108

Jessen, K.R., and R. Mirsky. 2005. The origin and development of glial cells in peripheral nerves. *Nat. Rev. Neurosci.* 6:671–682. http://dx.doi.org/10.1038/nrn1746

Kang, H., L. Tian, and W. Thompson. 2003. Terminal Schwann cells guide the reinnervation of muscle after nerve injury. *J. Neurocytol.* 32:975–985. http://dx.doi.org/10.1023/B:NEUR.0000020636.27222.2d

Kerschensteiner, M., M.E. Schwab, J.W. Lichtman, and T. Misgeld. 2005. In vivo imaging of axonal degeneration and regeneration in the injured spinal cord. *Nat. Med.* 11:572–577. http://dx.doi.org/10.1038/nm1229

Kerschensteiner, M., M.S. Reuter, J.W. Lichtman, and T. Misgeld. 2008. Ex vivo imaging of motor axon dynamics in murine triangularis sterni explants. *Nat. Protoc.* 3:1645–1653. http://dx.doi.org/10.1038/nprot.2008.160

Kirby, B.B., N. Takada, A.J. Latimer, J. Shin, T.J. Carney, R.N. Kelsh, and B. Appel. 2006. In vivo time-lapse imaging shows dynamic oligodendrocyte progenitor behavior during zebrafish development. *Nat. Neurosci.* 9:1506–1511. http://dx.doi.org/10.1038/nn1803

Kristan, W.B. Jr., F.J. Eisenhart, L.A. Johnson, and K.A. French. 2000. Development of neuronal circuits and behaviors in the medicinal leech. *Brain Res. Bull.* 53:561–570. http://dx.doi.org/10.1016/S0361-9230(00)00390-7

Lichtman, J.W., L. Magrassi, and D. Purves. 1987. Visualization of neuromuscular junctions over periods of several months in living mice. *J. Neurosci.* 7: 1215–1222.

Livet, J., T.A. Weissman, H. Kang, R.W. Draft, J. Lu, R.A. Bennis, J.R. Sanes, and J.W. Lichtman. 2007. Transgenic strategies for combinatorial expression of fluorescent proteins in the nervous system. *Nature*. 450:56–62. http://dx.doi.org/10.1038/nature06293

Lobsiger, C.S., and D.W. Cleveland. 2007. Glial cells as intrinsic components of non-cell-autonomous neurodegenerative disease. *Nat. Neurosci.* 10: 1355–1360. http://dx.doi.org/10.1038/nn1988

Love, F.M., and W.J. Thompson. 1998. Schwann cells proliferate at rat neuromuscular junctions during development and regeneration. *J. Neurosci.* 18: 9376–9385.

Mallon, B.S., H.E. Shick, G.J. Kidd, and W.B. Macklin. 2002. Proteolipid promoter activity distinguishes two populations of NG2-positive cells throughout neonatal cortical development. *J. Neurosci.* 22:876–885.

Marques, M.J., J.A. Conchello, and J.W. Lichtman. 2000. From plaque to pretzel: fold formation and acetylcholine receptor loss at the developing neuromuscular junction. *J. Neurosci.* 20:3663–3675.

McArdle, J.J., D. Angaut-Petit, A. Mallart, R. Bournaud, L. Faille, and J.L. Brigant. 1981. Advantages of the triangularis sterni muscle of the mouse for investigations of synaptic phenomena. *J. Neurosci. Methods*. 4:109–115. http://dx.doi.org/10.1016/0165-0270(81)90044-3

Mignone, J.L., V. Kukekov, A.S. Chiang, D. Steindler, and G. Enikolopov. 2004. Neural stem and progenitor cells in nestin-GFP transgenic mice. *J. Comp. Neurol.* 469:311–324. http://dx.doi.org/10.1002/cne.10964

Miledi, R., and C.R. Slater. 1968. Electrophysiology and electron-microscopy of rat neuromuscular junctions after nerve degeneration. *Proc. R. Soc. Lond. B Biol. Sci.* 169:289–306. http://dx.doi.org/10.1098/rspb.1968.0012

Miledi, R., and C.R. Slater. 1970. On the degeneration of rat neuromuscular junctions after nerve section. *J. Physiol.* 207:507–528.

Misgeld, T., M. Kerschensteiner, F.M. Bareyre, R.W. Burgess, and J.W. Lichtman. 2007. Imaging axonal transport of mitochondria in vivo. *Nat. Methods*. 4:559–561. http://dx.doi.org/10.1038/nmeth1055

Nave, K.A. 2010. Myelination and support of axonal integrity by glia. *Nature*. 468:244–252. http://dx.doi.org/10.1038/nature09614

Nedergaard, M., B. Ransom, and S.A. Goldman. 2003. New roles for astrocytes: redefining the functional architecture of the brain. *Trends Neurosci.* 26:523–530. http://dx.doi.org/10.1016/j.tins.2003.08.008

Nguyen, Q.T., J.R. Sanes, and J.W. Lichtman. 2002. Pre-existing pathways promote precise projection patterns. *Nat. Neurosci.* 5:861–867. http://dx.doi.org/10.1038/nn905

Nimmerjahn, A., F. Kirchhoff, and F. Helmchen. 2005. Resting microglial cells are highly dynamic surveillants of brain parenchyma in vivo. *Science*. 308:1314–1318. http://dx.doi.org/10.1126/science.1110647

Noakes, P.G., M. Gautam, J. Mudd, J.R. Sanes, and J.P. Merlie. 1995. Aberrant differentiation of neuromuscular junctions in mice lacking s-laminin/laminin beta 2. *Nature*. 374:258–262. http://dx.doi.org/10.1038/374258a0

O'Malley, J.P., M.T. Waran, and R.J. Balice-Gordon. 1999. In vivo observations of terminal Schwann cells at normal, denervated, and reinnervated mouse neuromuscular junctions. *J. Neurobiol.* 38:270–286. http://dx.doi.org/10.1002/(SICI)1097-4695(19990205)38:2<270::AID-NEU9>3.0.CO;2-F

Patton, B.L., A.Y. Chiu, and J.R. Sanes. 1998. Synaptic laminin prevents glial entry into the synaptic cleft. *Nature*. 393:698–701. http://dx.doi.org/10.1038/31502

Peles, E., M. Nativ, M. Lustig, M. Grumet, J. Schilling, R. Martinez, G.D. Plowman, and J. Schlessinger. 1997. Identification of a novel contactin-associated transmembrane receptor with multiple domains implicated in protein-protein interactions. *EMBO J.* 16:978–988. http://dx.doi.org/10.1093/emboj/16.5.978

Reddy, L.V., S. Koirala, Y. Sugiura, A.A. Herrera, and C.P. Ko. 2003. Glial cells maintain synaptic structure and function and promote development of the neuromuscular junction in vivo. *Neuron*. 40:563–580. http://dx.doi.org/10.1016/S0896-6273(03)00682-2

Reichenbach, A., A. Derouiche, and F. Kirchhoff. 2010. Morphology and dynamics of perisynaptic glia. *Brain Res. Brain Res. Rev.* 63:11–25. http://dx.doi.org/10.1016/j.brainresrev.2010.02.003

Reynolds, M.L., and C.J. Woolf. 1992. Terminal Schwann cells elaborate extensive processes following denervation of the motor endplate. *J. Neurocytol.* 21:50–66. http://dx.doi.org/10.1007/BF01206897

Rich, M.M., and J.W. Lichtman. 1989. In vivo visualization of pre- and postsynaptic changes during synapse elimination in reinnervated mouse muscle. *J. Neurosci.* 9:1781–1805.

Rossetto, O., M. Rigoni, and C. Montecucco. 2004. Different mechanism of blockade of neuroexocytosis by presynaptic neurotoxins. *Toxicol. Lett.* 149:91–101. http://dx.doi.org/10.1016/j.toxlet.2003.12.023

Sagasti, A., M.R. Guido, D.W. Raible, and A.F. Schier. 2005. Repulsive interactions shape the morphologies and functional arrangement of zebrafish peripheral sensory arbors. *Curr. Biol.* 15:804–814. http://dx.doi.org/10.1016/j.cub.2005.03.048

Sanes, J.R., and J.W. Lichtman. 1999. Development of the vertebrate neuromuscular junction. *Annu. Rev. Neurosci.* 22:389–442. http://dx.doi.org/10.1146/annurev.neuro.22.1.389

Scherer, S.S. 1996. Molecular specializations at nodes and paranodes in peripheral nerve. *Microsc. Res. Tech.* 34:452–461. http://dx.doi.org/10.1002/(SICI)1097-0029(19960801)34:5<452::AID-JEMT5>3.0.CO;2-O

Son, Y.J., and W.J. Thompson. 1995a. Nerve sprouting in muscle is induced and guided by processes extended by Schwann cells. *Neuron*. 14:133–141. http://dx.doi.org/10.1016/0896-6273(95)90247-3

Son, Y.J., and W.J. Thompson. 1995b. Schwann cell processes guide regeneration of peripheral axons. *Neuron*. 14:125–132. http://dx.doi.org/10.1016/0896-6273(95)90246-5

Song, J.W., T. Misgeld, H. Kang, S. Knecht, J. Lu, Y. Cao, S.L. Cotman, D.L. Bishop, and J.W. Lichtman. 2008. Lysosomal activity associated with developmental axon pruning. *J. Neurosci.* 28:8993–9001. http://dx.doi.org/10.1523/JNEUROSCI.0720-08.2008

Thaxton, C., A.M. Pillai, A.L. Pribisko, J.L. Dupree, and M.A. Bhat. 2011. Nodes of Ranvier act as barriers to restrict invasion of flanking paranodal domains in myelinated axons. *Neuron*. 69:244–257. http://dx.doi.org/10.1016/j.neuron.2010.12.016

Turney, S.G., and J.W. Lichtman. 2008. Chapter 11: Imaging fluorescent mice in vivo using confocal microscopy. *Methods Cell Biol.* 89:309–327. http://dx.doi.org/10.1016/S0091-679X(08)00611-0

van Mier, P., and J.W. Lichtman. 1994. Regenerating muscle fibers induce directional sprouting from nearby nerve terminals: Studies in living mice. *J. Neurosci.* 14:5672–5686.

Walsh, M.K., and J.W. Lichtman. 2003. In vivo time-lapse imaging of synaptic takeover associated with naturally occurring synapse elimination. *Neuron*. 37:67–73. http://dx.doi.org/10.1016/S0896-6273(02)01142-X

Watts, R.J., O. Schuldiner, J. Perrino, C. Larsen, and L. Luo. 2004. Glia engulf degenerating axons during developmental axon pruning. *Curr. Biol.* 14:678–684. http://dx.doi.org/10.1016/j.cub.2004.03.035

Williams, P.R., S.C. Suzuki, T. Yoshimatsu, O.T. Lawrence, S.J. Waldron, M.J. Parsons, M.L. Nonet, and R.O. Wong. 2010. In vivo development of outer retinal synapses in the absence of glial contact. *J. Neurosci.* 30:11951–11961. http://dx.doi.org/10.1523/JNEUROSCI.3391-10.2010

Zuo, Y., J.L. Lubischer, H. Kang, L. Tian, M. Mikesh, A. Marks, V.L. Scofield, S. Maika, C. Newman, P. Krieg, and W.J. Thompson. 2004. Fluorescent proteins expressed in mouse transgenic lines mark subsets of glia, neurons, macrophages, and dendritic cells for vital examination. *J. Neurosci.* 24:10999–11009. http://dx.doi.org/10.1523/JNEUROSCI.3934-04.2004